

# Exploring Cycle Consistency Learning in Interactive Volume Segmentation

Qin Liu<sup>1</sup>, Meng Zheng<sup>2</sup>, Benjamin Planche<sup>2</sup>, Zhongpai Gao<sup>2</sup>,  
Terrence Chen<sup>2</sup>, Marc Niethammer<sup>1</sup>, and Ziyang Wu<sup>2</sup>

<sup>1</sup> University of North Carolina at Chapel Hill

<sup>2</sup> United Imaging Intelligence, Cambridge MA, USA

<https://github.com/uncbiag/iSegFormer>

**Abstract.** Interactive volume segmentation can be approached via two decoupled modules: *interaction-to-segmentation* and *segmentation propagation*. Given a medical volume, a user first segments a slice (or several slices) via the interaction module and then propagates the segmentation(s) to the remaining slices. The user may repeat this process multiple times until a sufficiently high volume segmentation quality is achieved. However, due to the lack of human correction during propagation, segmentation errors are prone to accumulate in the intermediate slices and may lead to sub-optimal performance. To alleviate this issue, we propose a simple yet effective cycle consistency loss that regularizes an intermediate segmentation by referencing the accurate segmentation in the starting slice. To this end, we introduce a backward segmentation path that propagates the intermediate segmentation back to the starting slice using the same propagation network. With cycle consistency training, the propagation network is better regularized than in standard forward-only training approaches. Evaluation results on challenging benchmarks such as AbdomenCT-1k and OAI-ZIB demonstrate the effectiveness of our method. To the best of our knowledge, we are the first to explore cycle consistency learning in interactive volume segmentation.

## 1 Introduction

Medical image segmentation is a challenging yet critical task for various medical applications [1, 2], ranging from disease diagnosis [3, 4] to surgical planning and treatment [5, 6]. Although automated segmentation approaches have advanced significantly in recent years, they often deliver sub-optimal results without human corrections [7]. Instead, interactive segmentation allows users to refine automated segmentations with additional hints (*e.g.*, clicks [8], scribbles [9], and bounding boxes [10]), which turn out to be indispensable in various medical applications [7]. Therefore, growing efforts have been devoted to exploring interactive segmentation for medical images [7–11].

Highly successful temporal propagation modules have been proposed for semi-supervised video object segmentation (VOS) [12–14]. Inspired by these approaches, recent interactive volume segmentation methods [9, 11, 15] have

used a modular framework that decouples human interaction from segmentation propagation. In this way, a video temporal propagation module can be directly applied to medical volumes. Conceptually, these modular methods combine two tasks: interaction-to-segmentation (*i.e.*, interactive segmentation on 2D slices [8]) and segmentation propagation (*i.e.*, as in temporal propagation in semi-supervised VOS [13]). These modular methods differ significantly from unified 3D approaches [16, 17], which directly adopt 3D encoders and decoders for interactive volume segmentation. A strength of modular over unified approaches is that users can focus on segmenting a single slice to high quality without the need to check the effects of the interaction on other slices, as checking itself takes time and effort. Besides, modular methods provide more flexible support for different user interaction types as interaction and propagation are decoupled in training. Thus, we focus on modular interactive volume segmentation in this work.

The propagation module plays a critical role in existing modular interactive volume segmentation methods [9, 11, 15], which all rely on state-of-the-art Space Time Memory network (STM) [18] and its upgraded version Space Time Correspondence Network (STCN) [13] for propagation. STM builds a memory bank that stores representations for intermediate images and their segmentations. A query image then retrieves a segmentation from this memory bank by the learned correspondence between query and memory representations. STCN improves STM by introducing a much more memory-efficient correspondence learning approach. During training and inference, both STM and STCN use a sequential propagation order to support online processing in videos. However, this online restriction is unnecessary in medical volumes because they are usually acquired offline before segmentation. Besides, due to the lack of human correction, segmentation errors may accumulate in intermediate slices and may pollute the memory bank, leading to sub-optimal performance.

To alleviate this issue, we propose a simple yet effective cycle consistency loss that regularizes an intermediate segmentation by referencing an accurate segmentation in the starting slice. To this end, we introduce a backward segmentation path that propagates the intermediate segmentation back to the starting slice using the same propagation network. Compared with propagated segmentation of intermediate slices, the segmentation of the starting slice is always accurate and reliable. Therefore, segmentation errors of an intermediate slice flowing in a forward-backward loop will be alleviated by the accurate segmentation in the starting slice. We evaluated cycle consistency training on several public benchmarks, including AbdomenCT-1K [19] and OAI-ZIB [20]. Evaluation results on the AbdomenCT-1k dataset show that cycle consistency training improved segmentation on 8 out of 12 organs, including **24.9%** and **8.3%** improvements for the challenging esophagus and inferior vena cava, respectively. Our contributions are as follows:

- 1) We investigate the error accumulation problem of existing propagation modules for interactive volume segmentation and mitigate it by better training regularization.

- 2) We explore a simple yet effective cycle consistency training strategy that encourages self-correction for the intermediate propagated segmentations.
- 3) We evaluate our method on challenging and diverse benchmarks, demonstrating its effectiveness in improving propagation and segmentation quality.

## 2 Related Work

**Semi-Supervised Video Object Segmentation.** The goal of semi-supervised video object segmentation is to segment a video given the segmentation of the first frame [21]. We are particularly interested in approaches such as STM [18] and STCN [13] that build a memory bank for explicit pixel-level matching. STM was a breakthrough memory network that inspired many follow-up works such as SwiftNet [22] and STCN. Even though these memory networks were developed for videos, they have recently been applied for interactive segmentation on medical volumes [9, 11, 15]. However, all these methods share the same inherent limitation of memory networks that the propagation errors may accumulate in an increasing memory bank. *In this work, we explore using cycle consistency learning to mitigate this problem for the task of interactive volume segmentation.*

**Interactive Volume Segmentation.** Interactive volume segmentation remains challenging for medical images. Inspired by advancements in video object segmentation, researchers [9, 11, 15] have approached interactive volume segmentation with a modular framework that decouples human interaction from segmentation propagation. Mem3D [9] is the first modular method that applies STM [18] as the propagation network for interactive volume segmentation. It further proposes a quality assessment module to recommend the next slice for refinement. iSegFormer [15] uses STCN [13], an upgraded STM, as the propagation module. iSegFormer shows that the STCN model trained on videos can perform well on medical images even without finetuning. HybridNet [11] proposes a hybrid propagation network that combines STCN with a 3D encoder-decoder network to provide spatially-consistent features. HybridNet demonstrates that these features improve interactive segmentation performance. *In this work, we also use STCN as the propagation network due to its superior performance.*

**Cycle Consistency Learning in Computer Vision.** Cycle consistency learning is a general regularization mechanism that has been well-explored in various computer vision tasks such as video object segmentation [23], image synthesis [24], and unsupervised pretraining [25, 26]. In addition to applications in natural images, cycle consistency learning is also effective for medical image tasks. For instance, it has been applied to medical image segmentation [27], registration [28–30], and synthesis [31]. Note that cycle consistency learning itself is a general idea but not our contribution. Our main contribution is that we take the first step to explore cycle consistency learning in interactive volume segmentation. *More specifically, we aim to address the error accumulation problem in the propagation module by regularizing intermediate segmentations via a cyclic mechanism. In this regard, our work is significantly different from prior work.*

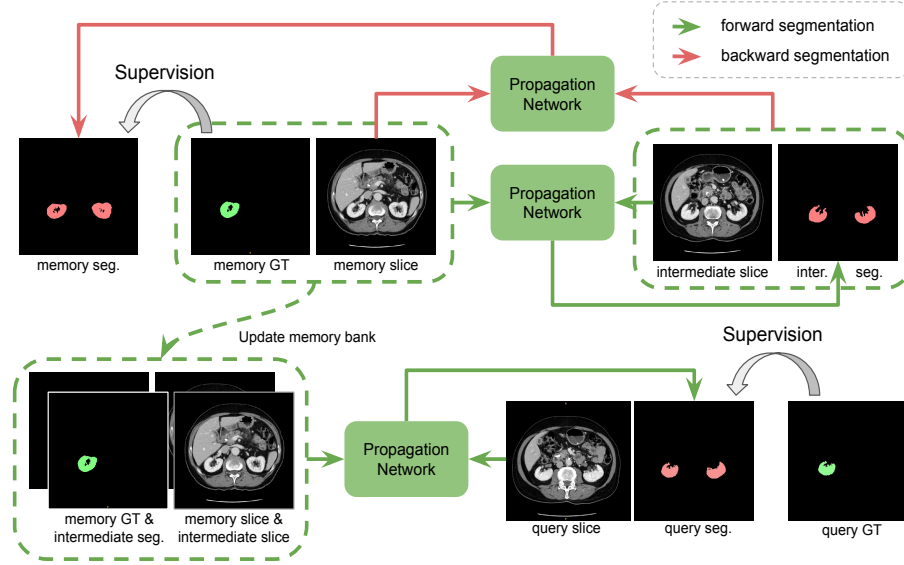


**Fig. 1.** Illustration of cycle consistency training. We use CT kidney segmentation as an example. We introduce a backward segmentation path (shown in red arrows) into a standard training process that consists of only forward segmentation paths (shown in green arrows). GT denotes ground truth (shown in green); seg. denotes model segmentation (shown in red). Weights are shared for the three propagation networks.

### 3 Cycle Consistency Learning

#### 3.1 Problem Formulation

Given a volume with  $T$  slices, a memory slice  $m$  is defined as the starting slice for propagation; a query slice  $q$  is defined as the target slice to be propagated; an intermediate slice  $p$  is defined as any slice that locates between  $m$  and  $q$ . Therefore, we have  $0 \leq id(m) < id(p) < id(q) \leq T - 1$ , where  $id(\cdot)$  returns the index of an input slice. The ground truth segmentations of slices  $m$ ,  $p$ , and  $q$  are denoted as  $m\_gt$ ,  $p\_gt$ , and  $q\_gt$ , respectively. A propagation network parameterized by  $\theta$  is denoted as  $net_\theta$ , which segments the intermediate slice following Eq. 1:

$$p\_seg = net_\theta(p, [m, m\_gt]) \quad (1)$$

where  $[\cdot]$  denotes a scalable memory bank that can be updated by appending more pairs of slice and segmentation. For example, to segment the query slice, the memory bank may be updated as  $[m, m\_gt, p, m\_seg]$  by appending the intermediate slice and its segmentation.

**Algorithm 1:** Pseudocode for calculating cycle consistency loss

---

```

# net: propagation network with learnable parameters
# loss: segmentation loss function (e.g., cross entropy loss)
# lambda: loss weight
# m, p, q: memory, intermediate, and query slices
# m_gt, q_gt: ground truths for memory and query slices

# forward segmentation
p_seg, q_seg = net(p, [m, m_gt]), net(q, [m, m_gt, p, p_seg])

# backward segmentation
m_seg = net(m, [q, q_seg])

# cycle loss
p_loss, q_loss = loss(p_seg, p_gt), loss(q_seg, q_gt)
m_loss = loss(m_seg, m_gt)
cycle_loss = p_loss + q_loss + lambda * m_loss

```

---

**3.2 Cycle Consistency Training**

For cycle consistency training, we randomly sample three slices (*i.e.* a memory slice  $m$ , an intermediate slice  $p$ , and a query slice  $q$  as defined in Sec. 3.1). The ground truth segmentations of the three slices are also provided. Fig. 1 shows the process of training a propagation network  $net_\theta$  (or  $net$  in short) via the three slices. In a nutshell, cycle consistency training introduces a backward segmentation path (shown in red arrows) into standard training that only performs forward segmentation (shown in green arrows). We introduce the details of forward and backward segmentation next.

**Forward Segmentation** There are two stages in forward segmentation: 1) the first stage propagates the memory ground truth  $m\_gt$  to the intermediate slice  $p$ , resulting in an intermediate segmentation  $p\_seg$ . This stage is denoted as  $p\_seg = net(p, [m, m\_gt])$ , in which the memory bank  $[m, m\_gt]$  only contains a memory slice and its ground truth. 2) the query slice then retrieves a segmentation via an updated memory bank  $[m, m\_gt, p, p\_seg]$ , which leverages the intermediate segmentation. This stage is denoted as  $q\_seg = net(q, [m, m\_gt, p, p\_seg])$ .

**Backward Segmentation** To further regularize the intermediate segmentation  $p\_seg$  obtained in forward segmentation, we propagate the intermediate segmentation  $p\_seg$  back to the memory slice  $m$  using the same propagation network  $net$ . Thus we obtain  $m\_seg$  and complete a propagation loop. The backward segmentation path can be denoted as  $m\_seg = net(m, [p, p\_seg])$ .

**3.3 Cycle Consistency Loss**

Given the segmentations from the forward and backward paths (described in Sec. 3.2), we define cycle consistency loss  $\mathcal{L}_{cycle}$  in Eq. 2:

$$\mathcal{L}_{cycle} = \mathcal{L}(p\_seg, p\_gt) + \mathcal{L}(q\_seg, q\_gt) + \lambda \mathcal{L}(m\_seg, m\_gt) \quad (2)$$

where  $\mathcal{L}$  denotes a conventional segmentation loss and  $\lambda$  controls the weight of memory segmentation loss. The intermediate segmentation  $p\_seg$ , the query segmentation  $q\_seg$ , and the memory segmentation  $m\_seg$  are all supervised by their corresponding ground truths using the same loss function  $\mathcal{L}$ . When  $\lambda = 0$ , our cycle consistency training degrades to the standard training. Alg. 1 shows the cycle consistency loss pseudo-code.

## 4 Experiments

**Datasets** We conduct our main experiments on AbdomenCT-1K [19] which contains 50 CT abdomen volumes (4794 slices) with manual segmentations for 12 diversified organs, including tiny and challenging organs such as the pancreas and esophagus, as well as large and regular organs such as the liver and kidney. We use the readily available video-pretrained weights for the propagation model for our experiments. Therefore, we only need a small amount of annotated data for finetuning, while leaving the majority of the data for evaluation. This dataset splitting is critical for medial volumes, where annotated volumes are scarce. Specifically, we split the AbdomenCT-1k dataset into 10 volumes (955 slices) for finetuning and 40 volumes (3839 slices) for testing. All 12 organs in the dataset are used for finetuning and testing. Therefore, these 12 organs are regarded as “seen” organs. To evaluate the model’s generalizability, we also generate rib segmentations for the testing volumes and use them as “unseen” organs for evaluation. Specifically, we generate two ribs (a left rib and a right rib) using our internally developed rib segmentation model with minor manual refinement. To evaluate the interactive volume segmentation performance, we also use 100 volumes from OAI-ZIB [20] dataset for femoral cartilage segmentation, following [15].

**Evaluation Protocol and Metrics** We evaluate each organ separately. For a specific organ, we select the slice with the largest organ area as the starting memory slice. We use the ground truth instead of the interactive segmentation results for propagation if not otherwise specified. This is for better comparison with propagation models without relying on the interaction module. We only conduct one round of propagation for simplicity and sufficiency to evaluate the propagation network. We report Region Jaccard ( $\mathcal{J}$ ), Boundary F measure ( $\mathcal{F}$ ), and their average ( $\mathcal{J\&F}$ ) to assess segmentation quality. We also report the Dice Similarity Coefficient (DSC) as an additional metric.

**Implementation Details** Our implementation is based on Python and PyTorch. Our models are trained and evaluated on an NVIDIA RTX A6000 GPU. We fix the number of finetuning iterations to 10k without model selection. We set  $\lambda = 0.1$  in the cycle consistency loss based on parameters tuning in videos. Other than this, we adopt most of the hyperparameters introduced in STCN [13] for a fair comparison with the baseline. For example, we follow the same data augmentation strategy that randomly reverses the order of the slices in a training batch; we also use bootstrapped cross entropy as the segmentation loss in Alg. 1 and Eq. 2.

	AbdomenCT-1K (seen)				Left Rib (unseen)				Right Rib (unseen)			
	$\mathcal{J}$	$\mathcal{F}$	$\mathcal{J}\&\mathcal{F}$	$DSC$	$\mathcal{J}$	$\mathcal{F}$	$\mathcal{J}\&\mathcal{F}$	$DSC$	$\mathcal{J}$	$\mathcal{F}$	$\mathcal{J}\&\mathcal{F}$	$DSC$
Baseline	56.0	74.3	66.1	71.8	27.4	45.2	36.3	43.0	23.3	36.9	30.1	37.8
+FT w/o Cycle	64.9	82.4	74.7	78.7	38.3	59.0	48.7	55.4	33.9	57.0	45.4	50.6
+FT w/ Cycle	<b>66.8</b>	<b>85.1</b>	<b>76.9</b>	<b>80.1</b>	<b>41.0</b>	<b>64.6</b>	<b>52.8</b>	<b>58.2</b>	<b>35.6</b>	<b>60.7</b>	<b>48.2</b>	<b>52.5</b>

**Table 1.** Propagation results on AbdomenCT-1k [19]. The baseline is a video-pretrained STCN [13] model without finetuning (FT). We observe that finetuning the baseline model significantly improves performance; finetuning with cycle consistency loss can further boost the performance, for both seen and unseen organs.

#### 4.1 Main Results

**Baseline** We use STCN [13] as our baseline model due to its state-of-the-art performance. It was pretrained on videos and can be directly applied to medical volumes. We finetune the baseline model w/ and w/o cycle consistency loss to demonstrate its effectiveness.

Tab. 1 shows evaluation results on the AbdomenCT-1k dataset. We compare three models: 1) a baseline model that was pretrained on videos without being finetuned on AbdomenCT-1k; 2) a finetuned baseline model without the cycle consistency learning; 3) a finetuned baseline model with cycle consistency learning. In addition to the 12 labeled organs (*i.e.*, “seen” organs), we generate the segmentations of ribs (*i.e.*, “unseen” organs) for the testing volumes to evaluate a model’s generalizability. All results in Tab. 1 are averaged over all volumes and all organs. First, we observe that finetuning an STCN model on medical images can significantly improve its performance. Second, our results show that cycle consistency learning can further boost the model’s performance, for both seen and unseen organs, demonstrating the benefits of our method. The relative improvement for each organ is shown in Fig. 2.

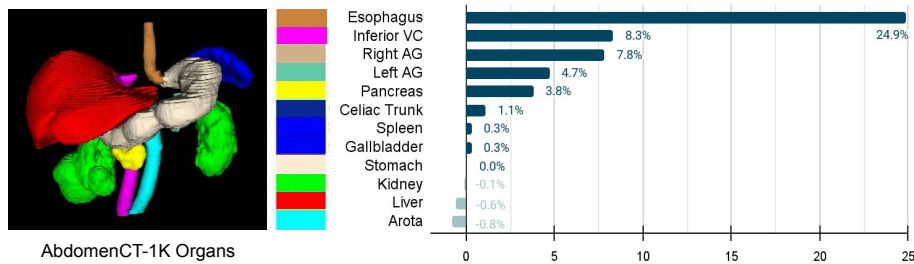


**Fig. 2.** Relative  $\mathcal{J}\&\mathcal{F}$  improvement on the AbdomenCT-1k dataset. Although the performance drops slightly for 3 organs, we observe improvements on 8 out of the full set of 12 organs, resulting in average improvements across all metrics (Tab. 1).

	round 1			round 3			round 5		
	click	scribble	oracle	click	scribble	oracle	click	scribble	oracle
AbdomenCT-1K	78.4	78.9	80.1	82.9	82.6	85.2	84.7	85.4	87.7
OAI-ZIB	69.7	69.5	71.8	77.5	77.1	79.9	80.7	80.1	82.5

**Table 2.** Results of interactive volume segmentation on AbdomenCT-1K [19] and OAI-ZIB [20] using different interactions. The metric is DSC.

## 4.2 Towards Interactive Volume Segmentation

In Sec. 4.1, we evaluated the propagation model in a one-round propagation setting in which the ground truth of the starting memory slice is provided. Here, our goal is to combine our best-performing propagation model with existing interactive segmentation models for interactive volume segmentation. Tab. 2 shows our results. We use SimpleClick [8] as the clicking model and S2M proposed in MiVOS [12] as the scribbling model. For the first propagation round, we pick the slice with the largest organ area for interactive segmentation and propagation. For the next rounds, we pick the slice with the worst segmentation to refine. We also use the ground truth for propagation as an oracle. No segmentation fusion [12] is conducted for simplicity. Fig 3 shows qualitative results for the first round propagation.

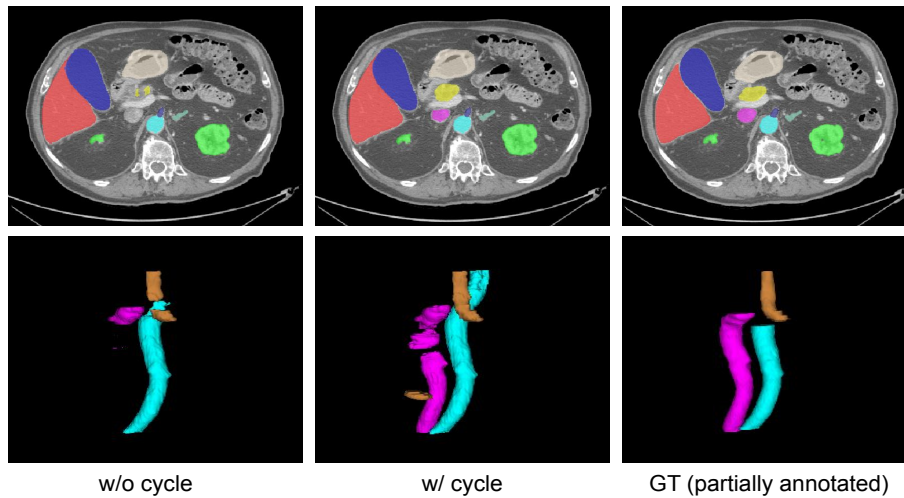


**Fig. 3.** Qualitative results for the first round propagation. As the ground truth for the Aorta (light blue) is not fully annotated at the top, our cycle consistency loss shows lower performance on the Aorta (Fig. 2) because it extends it beyond the annotation.



## 5 Conclusion

We took the first step to explore cycle consistency learning in interactive volume segmentation in order to alleviate the error accumulation problem in the propagation module. Specifically, we introduced a segmentation backward path and a cycle consistency loss that can be directly incorporated into the training process of existing works. Evaluation results on challenging and diversified benchmarks demonstrated the effectiveness of our method.

## References

1. D. Shen, G. Wu, and H.-I. Suk, “Deep learning in medical image analysis,” *Annual review of biomedical engineering*, vol. 19, pp. 221–248, 2017. [1](#)
2. G. Litjens, T. Kooi, B. E. Bejnordi, A. A. A. Setio, F. Ciompi, M. Ghafoorian, J. A. Van Der Laak, B. Van Ginneken, and C. I. Sánchez, “A survey on deep learning in medical image analysis,” *MedIA*, vol. 42, pp. 60–88, 2017. [1](#)
3. S. Devunooru, A. Alsadoon, P. Chandana, and A. Beg, “Deep learning neural networks for medical image segmentation of brain tumours for diagnosis: a recent review and taxonomy,” *Journal of Ambient Intelligence and Humanized Computing*, vol. 12, pp. 455–483, 2021. [1](#)
4. T. Heimann, B. J. Morrison, M. A. Styner, and M. Niethammer, “Segmentation of knee images: a grand challenge,” [1](#)
5. J. Li, M. Erdt, F. Janoos, T.-c. Chang, and J. Egger, “Medical image segmentation in oral-maxillofacial surgery,” *Computer-Aided Oral and Maxillofacial Surgery*, pp. 1–27, 2021. [1](#)
6. L. Soler, H. Delingette, G. Malandain, J. Montagnat, N. Ayache, C. Koehl, O. Dourthe, B. Malassagne, M. Smith, D. Mutter, *et al.*, “Fully automatic anatomical, pathological, and functional segmentation from CT scans for hepatic surgery,” *Computer Aided Surgery*, vol. 6, no. 3, pp. 131–142, 2001. [1](#)
7. G. Wang, W. Li, M. A. Zuluaga, R. Pratt, P. A. Patel, M. Aertsen, T. Doel, A. L. David, J. Deprest, S. Ourselin, *et al.*, “Interactive medical image segmentation using deep learning with image-specific fine tuning,” *IEEE TMI*, vol. 37, no. 7, pp. 1562–1573, 2018. [1](#)
8. Q. Liu, Z. Xu, G. Bertasius, and M. Niethammer, “SimpleClick: Interactive image segmentation with simple vision transformers,” *arXiv:2210.11006*, 2022. [1](#), [2](#), [8](#)
9. T. Zhou, L. Li, G. Bredell, J. Li, J. Unkelbach, and E. Konukoglu, “Volumetric memory network for interactive medical image segmentation,” *MedIA*, vol. 83, p. 102599, 2023. [1](#), [2](#), [3](#)
10. S. Zhang, J. H. Liew, Y. Wei, S. Wei, and Y. Zhao, “Interactive object segmentation with inside-outside guidance,” in *CVPR*, pp. 12234–12244, 2020. [1](#)
11. L. Shi, X. Zhang, Y. Liu, and X. Han, “A hybrid propagation network for interactive volumetric image segmentation,” in *MICCAI*, pp. 673–682, 2022. [1](#), [2](#), [3](#)
12. H. K. Cheng, Y.-W. Tai, and C.-K. Tang, “Modular interactive video object segmentation: Interaction-to-mask, propagation and difference-aware fusion,” in *CVPR*, pp. 5559–5568, 2021. [1](#), [8](#)
13. H. K. Cheng, Y.-W. Tai, and C.-K. Tang, “Rethinking space-time networks with improved memory coverage for efficient video object segmentation,” *NeurIPS*, vol. 34, pp. 11781–11794, 2021. [1](#), [2](#), [3](#), [6](#), [7](#)

14. H. K. Cheng and A. G. Schwing, “XMem: Long-term video object segmentation with an Atkinson-Shiffrin memory model,” in *ECCV*, pp. 640–658, 2022. [1](#)
15. Q. Liu, Z. Xu, Y. Jiao, and M. Niethammer, “isegformer: Interactive segmentation via transformers with application to 3D knee MR images,” in *MICCAI*, pp. 464–474, 2022. [1](#), [2](#), [3](#), [6](#)
16. A. Diaz-Pinto, P. Mehta, S. Alle, M. Asad, R. Brown, V. Nath, A. Ihsani, M. Antonelli, D. Palkovics, C. Pinter, *et al.*, “DeepEdit: Deep editable learning for interactive segmentation of 3D medical images,” in *MICCAI Workshop on Data Augmentation, Labelling, and Imperfections (DALI)*, pp. 11–21, 2022. [2](#)
17. X. Liao, W. Li, Q. Xu, X. Wang, B. Jin, X. Zhang, Y. Wang, and Y. Zhang, “Iteratively-refined interactive 3d medical image segmentation with multi-agent reinforcement learning,” in *CVPR*, pp. 9394–9402, 2020. [2](#)
18. S. W. Oh, J.-Y. Lee, N. Xu, and S. J. Kim, “Video object segmentation using space-time memory networks,” in *CVPR*, pp. 9226–9235, 2019. [2](#), [3](#)
19. J. Ma, Y. Zhang, S. Gu, C. Zhu, C. Ge, Y. Zhang, X. An, C. Wang, Q. Wang, X. Liu, S. Cao, Q. Zhang, S. Liu, Y. Wang, Y. Li, J. He, and X. Yang, “AbdomenCT-1K: Is abdominal organ segmentation a solved problem?,” *IEEE TPAMI*, 2021. [2](#), [6](#), [7](#), [8](#)
20. F. Ambellan, A. Tack, M. Ehlke, and S. Zachow, “Automated segmentation of knee bone and cartilage combining statistical shape knowledge and convolutional neural networks: Data from the osteoarthritis initiative,” *MedIA*, vol. 52, pp. 109–118, 2019. [2](#), [6](#), [8](#)
21. M. Gao, F. Zheng, J. J. Yu, C. Shan, G. Ding, and J. Han, “Deep learning for video object segmentation: a review,” *Artificial Intelligence Review*, vol. 56, no. 1, pp. 457–531, 2023. [3](#)
22. H. Wang, X. Jiang, H. Ren, Y. Hu, and S. Bai, “Swiftnet: Real-time video object segmentation,” in *CVPR*, pp. 1296–1305, 2021. [3](#)
23. Y. Li, N. Xu, J. Peng, J. See, and W. Lin, “Delving into the cyclic mechanism in semi-supervised video object segmentation,” *NeurIPS*, vol. 33, pp. 1218–1228, 2020. [3](#)
24. J.-Y. Zhu, T. Park, P. Isola, and A. A. Efros, “Unpaired image-to-image translation using cycle-consistent adversarial networks,” in *ICCV*, pp. 2223–2232, 2017. [3](#)
25. D. Dwibedi, Y. Aytar, J. Tompson, P. Sermanet, and A. Zisserman, “Temporal cycle-consistency learning,” in *CVPR*, pp. 1801–1810, 2019. [3](#)
26. X. Wang, A. Jabri, and A. A. Efros, “Learning correspondence from the cycle-consistency of time,” in *CVPR*, pp. 2566–2576, 2019. [3](#)
27. R. Wang and G. Zheng, “CyCMIS: Cycle-consistent cross-domain medical image segmentation via diverse image augmentation,” *MedIA*, vol. 76, p. 102328, 2022. [3](#)
28. B. Kim, D. H. Kim, S. H. Park, J. Kim, J.-G. Lee, and J. C. Ye, “CycleMorph: cycle consistent unsupervised deformable image registration,” *MedIA*, vol. 71, p. 102036, 2021. [3](#)
29. H. Greer, R. Kwitt, F.-X. Vialard, and M. Niethammer, “ICON: Learning regular maps through inverse consistency,” in *CVPR*, pp. 3396–3405, 2021. [3](#)
30. L. Tian, H. Greer, F.-X. Vialard, R. Kwitt, R. S. J. Estépar, and M. Niethammer, “GradICON: Approximate diffeomorphisms via gradient inverse consistency,” *arXiv preprint arXiv:2206.05897*, 2022. [3](#)
31. C. Wang, G. Macnaught, G. Papanastasiou, T. MacGillivray, and D. Newby, “Un-supervised learning for cross-domain medical image synthesis using deformation invariant cycle consistency networks,” in *MICCAI Workshop on Simulation and Synthesis in Medical Imaging (SASHIMI)*, pp. 52–60, 2018. [3](#)